Electrochimica Acta 128 (2014) 292–303

Contents lists available at ScienceDirect

Electrochimica Acta

journal homepage: www.elsevier.com/locate/electacta

The importance of ultrasonic parameters in the preparation of fuel cell catalyst inks

Bruno G. Pollet*, Jonathan T.E. Goh

South African Institute for Advanced Materials Chemistry (SAIAMC), Faculty of Natural Sciences, University of the Western Cape, Robert Sobukwe Road, Bellville 7535, Cape Town, South Africa

ARTICLE INFO

Article history:
Received 10 June 2013
Received in revised form
22 September 2013
Accepted 26 September 2013
Available online 19 October 2013

Keywords:
PEMFC
DMFC
Pt/C
Platinum
Catalyst Ink
Power ultrasound

ABSTRACT

We report here that ultrasound (20 kHz and 40 kHz) affects the catalyst ink composition when irradiated for longer periods and at high ultrasonic powers. In our study, two commercial carbon supported Pt (Pt/C) catalysts were used and dispersed in Nafion® ionomer. Catalyst ink samples prepared from Nafion®, IPA and water were either ultrasonicated (20 kHz up to 12.23 W and 40 kHz at 1.82 W) or mechanically shear-mixed (19,000 rpm) for various durations (up to 120 min). All catalyst ink samples were characterised by XRD, BET, TEM and electrochemical measurements were performed in liquid electrolytes. It was found that an optimised ultrasonic treatment is required to improve the catalytic ink activity, but longer irradiation is detrimental to its composition and morphology, mainly due to cavitation and sonolysis phenomena.

1. Introduction

There are numerous well-documented methods describing the preparation of PEMFC and DMFC catalyst inks. For example, Litster and McLean [1] and Wee et al. [2] give excellent overviews of PEMFC catalyst ink and electrode fabrication methods. It is common for catalyst inks to be mixed ultrasonically for a few minutes or hours (typically by immersion in laboratory ultrasonic cleaning baths in the range of 38–40 kHz) in order to produce a homogeneous mixture of carbon-supported Pt catalyst and ionomer binder, which is essential in order to maximise catalyst utilisation at the 'three-phase reaction zone' (also known as the Triple Phase Boundary – TPB).

For the last 20 years, there have been a few reports on the use of ultrasound for fabricating noble metal nanoparticles, catalysts and other fuel cell materials. Pollet [3] showed in his comprehensive review that the ultrasonic, sonochemical and sono-electrochemical methods used for the preparation of *mono*- and *bi*-metallic nanoparticles, carbon-supported electrocatalysts (via the ultrasonic functionalisation of the carbonaceous material), fuel cell electrodes and membranes offer unique and often highly advantageous experimental conditions by virtue of ultrasound-induced cavitation, water sonolysis and enhanced mass transport phenomena.

Ultrasound is defined as a sound wave with a frequency above 16 kHz with the upper limit usually taken to be 5 MHz for gases and 500 MHz for liquids and solids [4]. The application of ultrasound in chemical, physical and biological sciences can be divided into two main groups: (i) low frequency or power ultrasound (20–100 kHz) and (ii) high frequency or diagnostic ultrasound (2–10 MHz). Diagnostic ultrasound is often used in chemical analysis, medical scanning and in the study of relaxation phenomena [4]. Low amplitude waves are often used to determine the velocity and absorption coefficient of the sound wave by the medium, i.e. the effect of the medium on the ultrasonic wave. However, power ultrasound can be regarded as the effect of the sound wave on the medium. Low frequency and high energy waves are used in ultrasonic cleaning, drilling, soldering, chemical processes and emulsification [4].

Over the past few years the use of power ultrasound has found wide applications in the chemical and processing industries where it is used to enhance both synthetic and catalytic processes and to generate new products. This area of research has been termed *sonochemistry*, which mainly concerns reactions involving a liquid leading to an increase in reaction rates, product yields and erosion of surfaces [4]. However, the main reason for most of the observed effects of ultrasound on surfaces and chemical reactions is recognised as being due to 'cavitation' effect which occurs as a

* Corresponding author. Tel.: +27 0714840323.
E-mail address: bgpollet@uwc.ac.za (B.G. Pollet).
URLs: http://www.polleteresearch.com (B.G. Pollet), http://www.uwc.ac.za (B.G. Pollet).

0013-4686/$ – see front matter © 2014 Elsevier Ltd. All rights reserved.
http://dx.doi.org/10.1016/j.electacta.2013.09.160

secondary effect when an ultrasonic wave passes through a liquid medium.

Cavitation was first reported in 1895 by Thorneycroft and Barnaby [5] when they observed that the propeller of a submarine eroded over short operating times, caused by collapsing bubbles induced by hydrodynamic cavitation in turn generating intense pressure and temperature gradients locally. In the late 1920s, Rayleigh [6] published the first mathematical model describing 'cavitation' in incompressible fluids. It was not until 1927 that the use of ultrasound on chemical and biological systems was first observed and recognised as a useful tool by Richard and Loomis [7].

Cavitation is a phenomenon where microbubbles are formed which tend to implode and collapse violently in the liquid leading to the formation of high velocity jets of liquid. Indeed, ultrasound consists of alternating compression and rarefaction cycles (Fig. 1). During rarefaction cycles, negative pressures developed by the high power ultrasound are strong enough to overcome the intermolecular forces binding the fluid. The succeeding compression cycles can cause the microbubbles to collapse almost instantaneously with the release of a large amount of energy. Bubble formation is a three-step process consisting of nucleation, bubble growth and collapse of gas vapour filled bubbles in a liquid phase. These bubbles transform the low energy density of a sound field into a high energy density sound field by absorbing energy from the sound waves over one or several cycles and releasing it during very short intervals. Cavitation phenomenon is known to cause erosion, emulsification, molecular degradation, sonoluminescence and sonochemical enhancements of reactivity solely attributed to the collapse of cavitation bubbles [4]. It is now well accepted in the field that the cavitation bubble collapse leads to near adiabatic heating of the vapour that is inside the bubble, creating the so-called "hot-spot" in the fluid, where:

(1) High temperatures (ca. 5000 K) and high pressures (ca. 2000 atms) are generated with cooling rates of 10^{9-10} K s^{-1} during the collapsing of cavitation bubbles are observed. Here, water vapour is 'pyrolyzed' into hydrogen radicals ($H^{\bullet}$) and hydroxyl radicals ($OH^{\bullet}$), known as water sonolysis (Fig. 1).
(2) The interfacial region between the cavitation bubbles and the bulk solution is paramount. The temperature is lower in the interior of the bubbles than the exterior but high enough for thermal decomposition of the solutes to take place with greater local hydroxyl radical concentrations in this region.
(3) The reactions of solute molecules with hydrogen atoms and hydroxyl radicals occur in the bulk solution at ambient temperature.

Because of ultrasound's 'extraordinary' effects, extensive work has been carried out in which high power ultrasound (20 kHz to 2 MHz) was applied to various chemical processes leading to several industrial applications and many publications over a wide range of subject areas [4]. It has been shown that the effects of high intensity ultrasonic irradiation on chemical processes lead to both chemical and physical effects, for example, mass-transport enhancement, surface cleaning and radical formation via sonolysis due to cavitation phenomena (Fig. 2) [4].

Our own literature search revealed that nearly 90% of low temperature fuel cell catalyst ink preparations use ultrasound (usually ultrasonic cleaning baths) for the efficient dispersion and homogenisation of the catalyst inks prior to PEMFC and DMFC electrode fabrication. In some cases, the literature indicates that: (i) the ultrasound source type (horn or bath), ultrasonic frequency, power, intensity and irradiation time are not reported, and (ii) temperature is not often controlled, regulated and reported (it is well-known that power ultrasound yields rapid temperature rises with ΔTs of up to ~+50 °C in short exposure times e.g. up to 1 hour in water starting from room temperature). In other cases, ultrasound time is mentioned and varies from 5 min to 24 h ultrasonication from one study to another.

Two fairly recent papers published by Takahashi and Kocha [8] and Garsany et al. [9] describe the importance of catalyst ink optimisation when evaluating electrocatalysts activities towards the ORR (Oxygen Reduction Reaction) in liquid electrolytes using the RDE (Rotating Disc Electrode) methodology. The authors highlighted the importance of producing good dispersion with the catalyst ink prior to deposition on an electrode. Good catalyst ink dispersions were qualitatively identified by ultrasonicating the catalyst ink and allowing it to rest without stirring for a period of time. Electrochemical Surface Area (*ECSA*) was used as the quantitative parameter in order to decide whether the catalyst ink dispersion was optimal. For their baseline Pt/C (C: Vulcan XC-72R) catalyst, their study showed an increase in the *ECSA* from 80 to 100 m^2 g^{-1} (25%) whereas for their Heat-Treated (HT) Pt/C-HT catalyst an even more drastic variation was observed (35–74 m^2 g^{-1}). They observed that the important factor in the catalyst ink optimisation was the ratio of IPA to water (found to be ~35%) in the catalyst ink formulation as well as the energy and duration of the subsequent ultrasonic treatment. It was observed that for a given catalyst ink composition, ultrasonication times of less than 5 min showed irreproducible results, and durations greater than 10–15 min were found to be sufficient for all the catalyst inks studied. Beyond 15 min and for up to a period of 3 h, the effect of continued ultrasonication was found to produce no observable degradation in terms of loss in *ECSA* or particle growth in TEM, indicating a reasonably strong adhesion of Pt to the carbon support.

In this paper, we report for the first time a systematic study of the effects of ultrasound on the performance of the catalyst ink. *ECSAs* are compared for catalyst inks prepared in the absence (silent) and presence of ultrasound, at various ultrasonic frequencies, powers and exposure times. In this study and in our conditions, we observed a decrease in *ECSA* for catalyst ink samples when treated for longer irradiation times at the two ultrasonic frequencies employed. Herein, possible degradation mechanism(s) are proposed (assuming that the Nafion® is not affected by ultrasound).

Note that the authors have recently shown that ultrasonication of Nafion® solutions over various irradiation times revealed a decrease in viscosity. However, it was found that at a minimum ultrasonic time and a fixed ultrasonic frequency, an increase in Nafion® polymer viscosity was also observed. This observation was mainly attributed to the fact that depolymerisation caused by ultrasound, supplies new chain carriers for polymerisation, in other words under carefully chosen conditions, ultrasound may initiate polymerisation as previously observed in other studies using various polymers [10–16].

2. Experimental methods

2.1. Materials

In this study, two commercial catalysts were used as supplied by Tanaka Kikinzoku Kogyo (TEC10E50E; 45.9 wt% Pt/C TKK, Japan) and *E-Tek* (HP ~50 wt% Pt/C, USA). Nafion® dispersion (10 wt%, EW 1100, D1021, DuPont), isopropanol (IPA, AR, Fisher) and ultrapure water (18.2 MΩ Millipore) were used for catalyst ink preparation. All gases used in these experiments were of ultra-high purity research grades (BOC, England).

2.2. Catalyst Inks preparation

The catalyst inks were prepared by mixing commercial Pt/C (C: Vulcan XC-72R) with Nafion® solution and IPA to form a

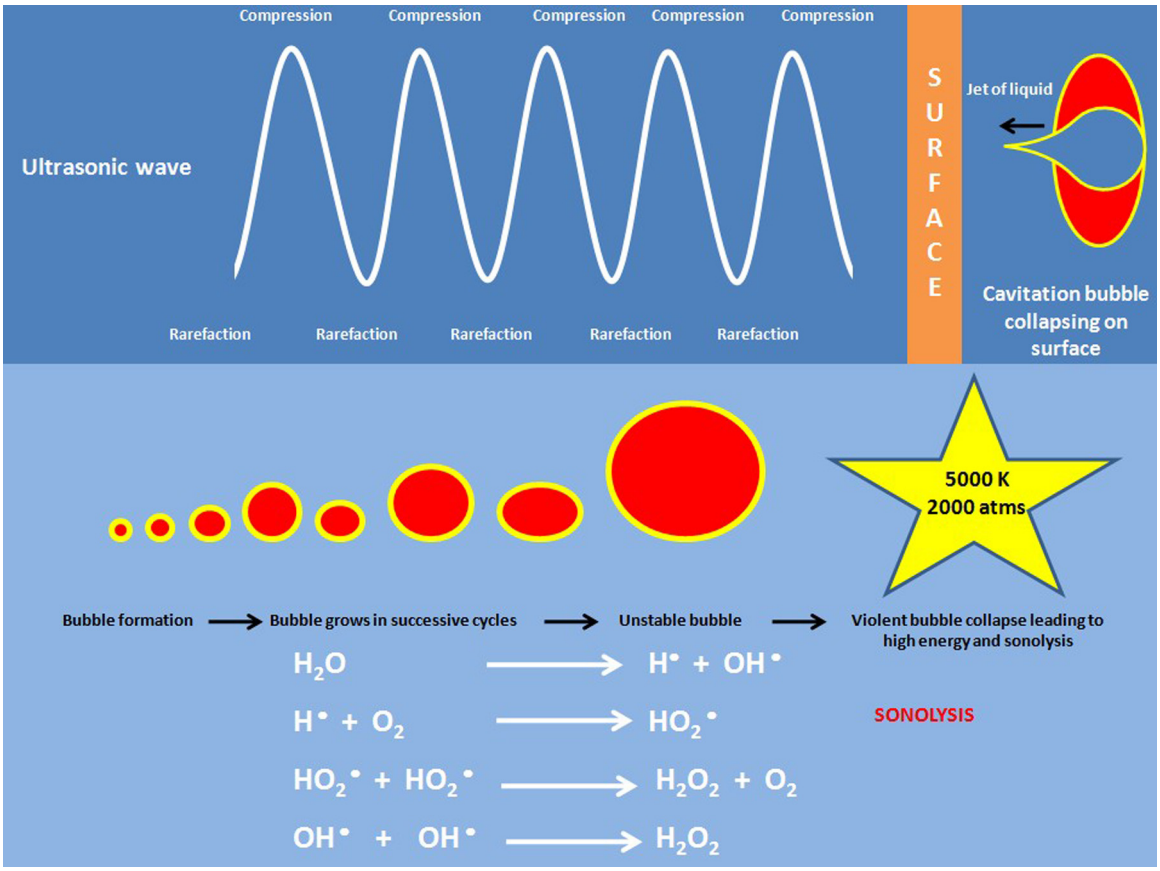

Fig. 1. Cavitation bubble formation at various stages during alternating compression and rarefaction cycles of the ultrasonic wave and asymmetric bubble collapse on a surface leading to (i) high energy with temperature up to 5000 K and pressure of up to 2000 atm and (ii) the sonolysis of water caused by the high energy where $OH^\bullet$ are hydroxyl radicals, $HO_2^\bullet$ are perhydroxyl radicals and H_2O_2 is hydrogen peroxide.

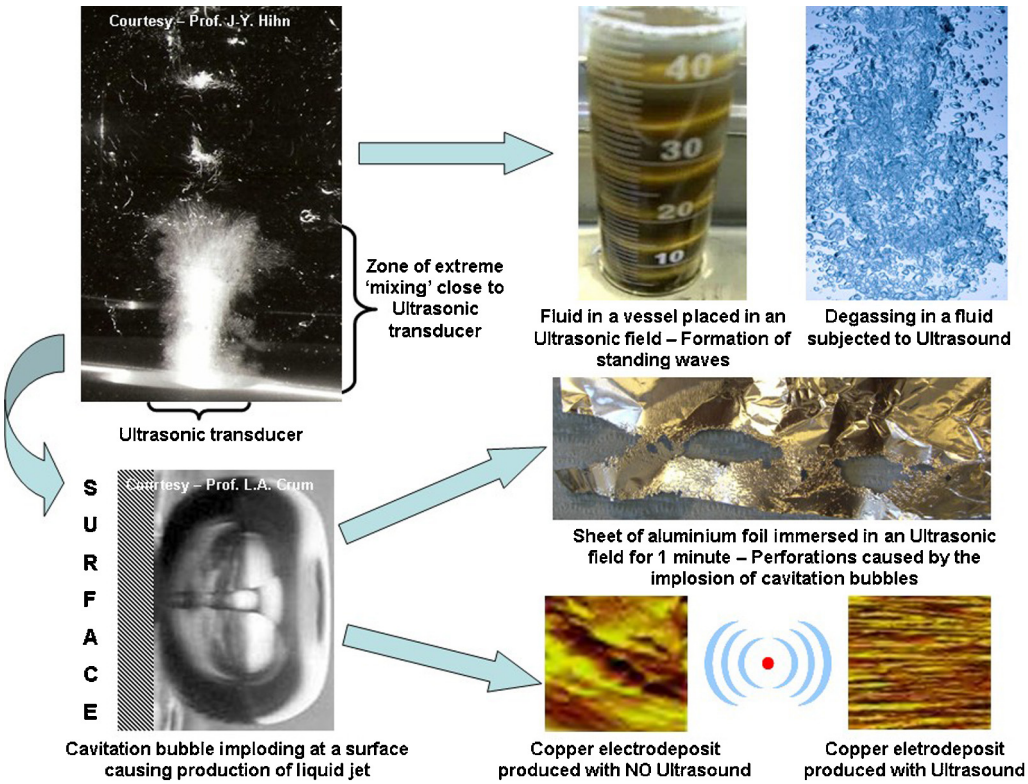

Fig. 2. Effects of high intensity ultrasonic irradiation on chemical processes leading to both chemical and physical effects: mass-transport enhancement, erosion, surface cleaning and radical formation via sonolysis due to cavitation phenomena.

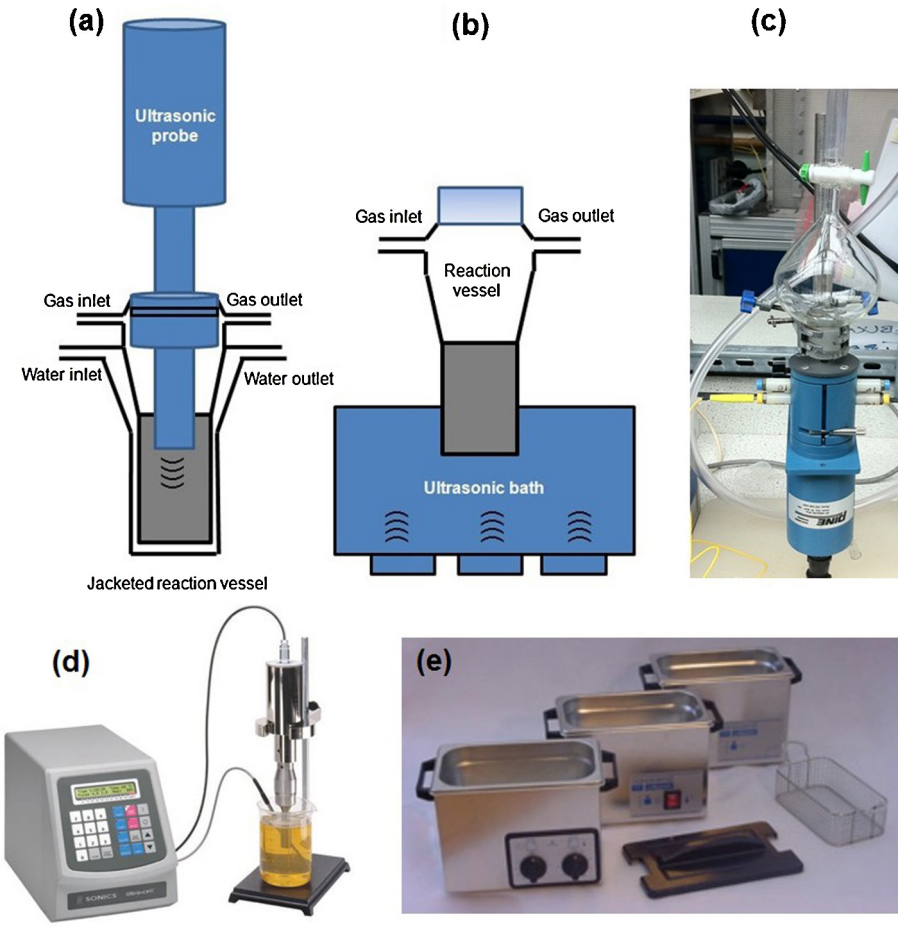

Fig. 3. (a) Ultrasonic probe (20 kHz); (b) ultrasonic bath (40 kHz); (c) inverted Rotating Disc Electrode (RDE) operating at 50 rpm under Ar atmosphere for the preparation of thin-film electrodes; (d) 20 kHz Vibra-Cell VCX750 ultrasound probe with an ultrasonic generator/processor (Sonics & Materials Inc., USA); (e) 40 kHz Ultrasonic 375H series (Langford Electronics Ltd., Coventry, UK).

well-dispersed ink. 5 mg of the commercial Pt/C catalyst was first weighed into a vial and 5.14 ml of ultrapure water, 28 μL of Nafion® and 1.62 ml IPA were added. The final solution was then hand-shaken vigorously for 5 min to produce a *Pt/C/Nafion®* solution and immediately either ultrasonicated using an ultrasonic bath or probe, or mechanically homogenised using a high-shear mixer.

2.3. Ultrasonication of the catalyst inks

Catalyst ink samples (V = 7 ml) were ultrasonicated for various durations (t = 0, 10, 30, 60 and 120 min) at (298 ± 1) K using either an ultrasonic probe [20 kHz Vibra-Cell VCX750 with a tip diameter of 6 mm (Sonics & Materials Inc.), Fig. 3(a)] or a thermostatic ultrasonic bath [40 kHz Ultrasonic 375H (Langford Electronics Ltd., Coventry, UK), Fig. 3(b)]. For the 20 kHz and 40 kHz experiments, the catalyst inks were either added in a sealed glass vial (positioned in the middle of the ultrasonic bath and at a distance of 7 cm from the ultrasonic transducers (situated at the bottom of the bath) to give maximum ultrasonic agitation – the positioning of the vial was achieved either by using the 'aluminium foil' or the 'Ferri/Ferrocyanide' tests as described in [4,17]) or inserted in a sealed jacketed reaction vessel linked to a thermostatic bath, respectively. Characterisation of the catalyst ink samples was performed immediately following ultrasonication.

2.4. High shear mixing of the catalyst inks

For completeness and to separate the effects of cavitation from mixing induced by ultrasound, all catalyst inks were subjected to mechanical mixing in the absence of ultrasound. Catalyst ink samples (V = 7 ml) were mixed in a vessel for various durations (t = 0, 10, 30, 60 and 120 min) at (298 ± 1) K using a high-shear mixer (Heidolph Silent Crusher) operating at 19,000 rpm with a rotor diameter of 3.2 mm. The high-shear mixer blade was positioned in the middle of the vessel and immersed at a depth of 2 cm in the catalyst ink sample. Characterisation of catalyst ink samples was performed immediately following mixing.

2.5. Electrochemical measurements

Glassy carbon (GC, Radiometer Analytical or Pine Instruments) disc electrodes (⌀ = 3 mm) embedded in a Teflon cylinder were used. The GC electrodes were polished to a mirror finish with polishing paper (Buelher-Met, P600) and 1.0 μm, 0.3 μm down to 0.05 μm alumina oxide paste (Al_2O_3), cleaned by ultrasonication in ultrapure water (R = 18.2 MΩ) using the ultrasonic bath (40 kHz) for 1 min to remove any traces of contaminants. The GC electrodes were dried with argon, then in a vacuum oven.

For all electrochemical characterisations, working electrodes (GC) were prepared by pipetting an aliquot of catalyst ink (3.8 μl for *E-TEK* and 4.0 μl for *TKK* catalyst inks) onto the 3 mm GC electrode to achieve a Pt loading of 20 μg cm^{-2}. The GC/Pt/C/Nafion® electrodes were subjected to a strict drying procedure whereby the catalyst ink was mounted on an inverted Rotating Disc Electrode (RDE) rotating at 200 rpm under a stream of nitrogen or argon to yield good, uniform and reproducible thin-films [Fig. 3(c)].

Table 1
Average diameters, physical surface areas (*S*), electrochemical surface areas (*ECSA*) and utilisations for the *E-tek* ~50 wt% Pt/C catalyst under silent, high shear mixed (19,000 rpm) and ultrasonicated conditions (20 kHz and 40 kHz) at various ultrasonic powers and selected irradiation times. The table also shows average diameters and physical surface areas (*S*) of Pt for pristine *E-tek* ~50 wt% Pt/C catalyst powders determined by XRD and TEM.

E-TEK ~50 wt% Pt/C (C: Vulcan XC-72R)				
	Avg. diameter (Sauter)/nm	Physical surface area (*S*)[a]/$m^2\ g^{-1}$	*ECSA*(*Pt*)/$m^2\ g^{-1}$	Utilisation[b]/%
Pristine (XRD)	7.20	39.51	–	–
Pristine (TEM)	3.94	72.15	–	–
Bath (30 min, 1.82 W)	3.91	72.85 ± 0.10	82.78	112.50
Bath (60 min, 1.82 W)	4.20	67.78 ± 5.11	70.32	111.80
Probe (10 min, 3.03 W)	3.81	74.73 ± 1.97	70.20	96.23
Probe (5 min, 6.70 W)	3.98	71.48 ± 1.92	57.94	83.29
Probe (120 min, 12.23 W)	5.38	52.88 ± 2.47	54.25	97.53
High shear mixer (120 min, 19,000 rpm)	3.62	78.62 ± 7.08	45.24	57.54

[a] Errors arising from analysis of TEM images.
[b] Given by Utilisation (*U*) = (*ECSA*/*S*) × 100%.

All electrochemical experiments were conducted using the methods described by Gasteiger et al. [18], Takahashi and Kocha [8], Curnick et al. [19] and Garsany et al. [9] and performed at (298 ± 1) K in a 3-electrode cell set up in a Faraday cage, using an Autolab PGSTAT302 N potentiostat (Eco-Chemie) and a RDE setup (ED101, Radiometer Analytical or Pine Instruments). The background electrolyte was 0.1 M double distilled ultrapure perchloric acid ($HClO_4$) prepared from 70% (TraceSelect, Sigma). The counter and the reference electrodes were Pt gauze and a home-made Reversible Hydrogen Electrode (RHE), respectively. Herein, all potentials are quoted with respect to RHE. All glassware was subjected to a rigorous cleaning procedure involving soaking in a 1:1 sulfuric acid and nitric acid mixture overnight, followed by thoroughly rinsing and boiling in ultrapure water to ensure minimal residual impurities.

Before *ECSA* experiments, the solutions were deoxygenated by bubbling nitrogen for 20 min and then the electrode was conditioned by potential cycling for 50 cycles between +0.05 V and +1.1 V vs. RHE at 250 mV s^{-1}. Cyclic voltammograms (CVs) were recorded at 25 mV s^{-1} between +0.05 V and +1.1 V vs. RHE under nitrogen atmosphere. The *ECSA* values in $m^2\ g^{-1}$ were determined according to Eq. (1) [19] after the subtraction of capacitive currents:

$$ECSA = \frac{Q_{Hupd} \cdot 100}{210 \cdot W_{Pt} \cdot A} \quad (1)$$

where Q_{Hupd} (μC) is the charge measured upon desorption of a monolayer of underpotentially-deposited (UPD) hydrogen (Q_{Hupd}) region (+0.05 to +0.4 V vs. RHE), W_{Pt} is the Pt loading (μg cm^{-2}), *A* is the geometric area of the GC (cm^2) and the value 210 μC cm^{-2} corresponds to the charge passed during hydrogen UPD on a bulk polycrystalline Pt surface. All *ECSA* measurements were repeated at least three times.

2.6. Physical characterisation

XRD analysis of dry Pt/C catalyst powders was performed using an X-ray diffractometer (Bruker D8 ADVANCE) operating with Cu Kα radiation (λ = 0.15406 nm) generated at 40 kV and 40 mA. The volume-averaged particle size was calculated from the full width half-maximum of the (1 1 1) peak using the Scherrer equation [20]:

$$d = \frac{k \cdot \lambda}{\beta \cdot \cos\theta} \quad (2)$$

where *d* is the average particle size in Å, *k* is a shape-sensitive coefficient (0.9, assuming spherical particles), λ the wavelength of radiation used (1.54056 Å), β is the full width half maximum of the peak in radian and θ is the angle at the position of peak maximum in radian [20].

Specific surface areas of dry Pt/C catalyst powders were measured by the *BET* method (Brunauer, Emmett and Teller, 1938) using Octane adsorption in Dynamic Vapour Sorption (DVS, Surface Measurement Systems Ltd, UK), providing the total physical surface area of Pt and carbon. The *BET* values for the *E-TEK* ~50 wt% Pt/C (C: Vulcan XC-72R) and *TKK* TEC10E50E ~46 wt% Pt/C (C: Vulcan XC-72R) were 93.49 ± 4.59 $m^2\ g^{-1}$ and 239.30 ± 7.10 $m^2\ g^{-1}$ respectively, which is in fairly good agreement with previous findings [8,9,18,19].

TEM analysis was carried out using a JEOL 1200ex Transmission Electron Microscope operating at 300 kV. Histograms of particle size were constructed from images by measuring at least 150 particles using ImageJ software. The Pt surface area *S* ($m^2\ g^{-1}$) was estimated according to mean particle size using Eq. (3) [21],

Table 2
Average diameters, physical surface areas (*S*), electrochemical surface areas (*ECSA*) and utilisations for the *TKK* TEC10E50E ~46 wt% Pt/C catalyst under silent, high shear mixed (19,000 rpm) and ultrasonicated conditions (20 kHz and 40 kHz) at various ultrasonic powers and selected irradiation times. The table also shows average diameters and physical surface areas (*S*) of Pt for pristine *TKK* TEC10E50E ~46 wt% Pt/C catalyst powders determined by XRD and TEM.

TKK TEC10E50E ~46 wt% Pt/C (C: Vulcan XC-72R)				
	Avg. diameter (Sauter)/nm	Physical surface area (*S*)[a]/$m^2\ g^{-1}$	*ECSA*(*Pt*)/$m^2\ g^{-1}$	Utilisation[b]/%
Pristine (XRD)	4.10	69.39	–	–
Pristine (TEM)	3.00	94.79	–	–
Bath (30 min, 1.82 W)	2.93	96.94 ± 2.18	89.05	91.86
Bath (60 min, 1.82 W)	3.50	81.24 ± 0.87	79.13	97.41
Probe (10 min, 3.03 W)	3.12	91.26 ± 6.5	99.40	108.92
Probe (5 min, 6.70 W)	3.08	92.46 ± 6.51	100.71	108.92
Probe (120 min, 12.23 W)	3.00	94.73 ± 3.83	92.50	97.64
High shear mixer (120 min, 19,000 rpm)	3.12	91.23 ± 7.05	84.05	92.13

[a] Errors arising from analysis of TEM images.
[b] Given by Utilisation (*U*) = (*ECSA*/*S*) × 100%.

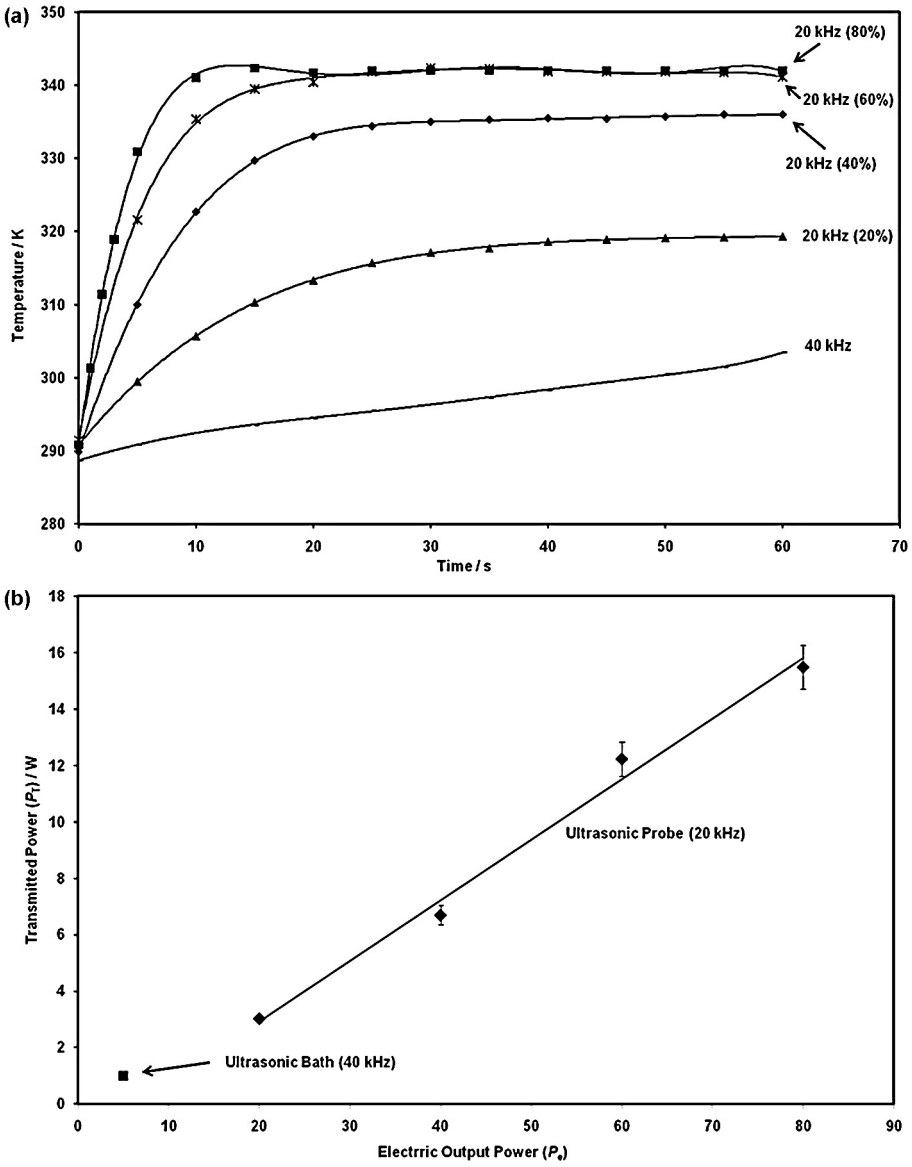

Fig. 4. (a) Plots of *temperature* vs. *time* at various electric output powers using the ultrasonic bath (40 kHz) and probe (20 kHz); (b) plot of *transmitted ultrasonic power* (P_T) vs. *electric output power* (P_e).

assuming that all Pt particles in the samples are available and represent spheres with diameter d:

$$S = \text{surface area/mass} = \frac{\pi d^2}{1/6\pi d^3 \rho} = \frac{6 \cdot 10^3}{\rho \cdot d} = \frac{280}{d} \quad (3)$$

where ρ is the platinum density (21.4 g cm^{-3}) and d is the Sauter average particle diameter (nm) [21].

Using Eq. (3) and TEM images of the dry powder catalysts (not shown here), a measured average particle size of 3.9 nm for the *E-TEK* ~50 wt% Pt/C and *TKK* TEC10E50E ~46 wt% of 3 nm would correspond to a specific surface area of 72 m^2 g^{-1} and 95 m^2 g^{-1} respectively (Tables 1 and 2).

3. Results and discussion

3.1. Ultrasonic power determination

The ultrasonic power dissipated (P_T) in the samples by the ultrasonic equipment was determined calorimetrically according to the procedure of Mason et al. [22,23] and Margulis and Margulis [24].

In these experiments temperature (T) was recorded every 5 s over a period of 1 min (t) using a thermocouple fitted to a Fluke 51 digital thermometer. Experimental temperature (T in K) was plotted against time (t in s) and a curve fitting analysis was performed. Here, in our conditions, T vs. t plots were found to be a 6th order polynomial in the form of:

$$T = a + bt + ct^2 + dt^3 + et^4 + ft^5 + gt^6 \quad (4)$$

Differentiation of Eq. (4) yields Eq. (5)

$$\frac{dT}{dt} = b + 2ct + 3dt^2 + 4et^3 + 5ft^4 + 6gt^5 \quad (5)$$

$$\text{for which at } t = 0, \text{ Eq. (5) gives } \left(\frac{dT}{dt}\right)_{t=0} = b \quad (6)$$

The ultrasonic power (P_T) is then determined as:

$$P_T = m_{ci}.C_{p(ci)} \cdot \left(\frac{dT}{dt}\right)_{t=0} \quad (7)$$

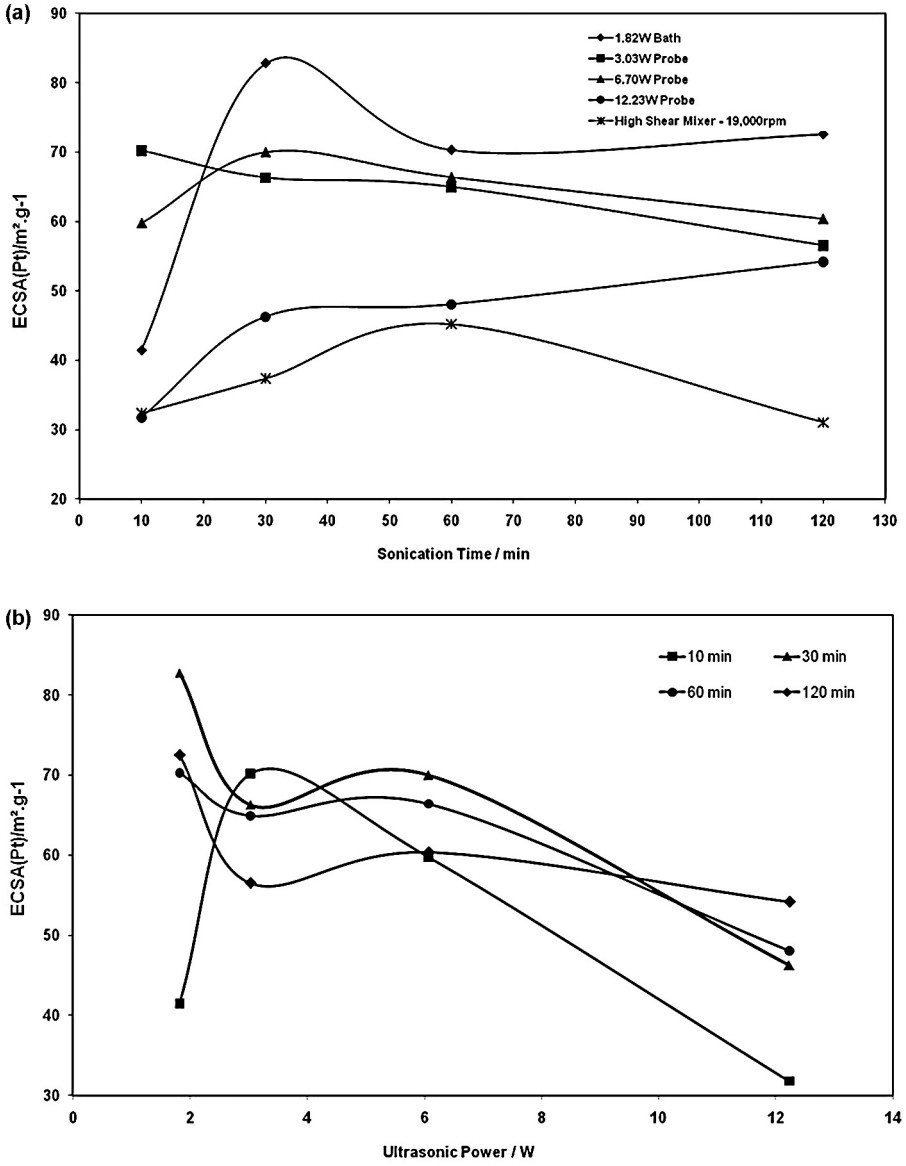

Fig. 5. (a) Plots of *ECSAs* vs. *ultrasonication time* at two ultrasonic frequencies (20 and 40 kHz), at various ultrasonic powers and for high-shear mixing (19,000 rpm, no ultrasound – silent) for the *E-TEK* samples – *ECSA* values (at least 3 replicates) were determined from cyclic voltammograms experiments recorded at 25 mV s^{-1} in 0.1 M $HClO_4$ (not shown here) and at (298 ± 1) K, (b) plots of *ECSAs* vs. *ultrasonic powers* at various ultrasonication times for the *E-TEK* samples.

where P_T is the transmitted ultrasonic power in W; m_{ci} is the mass of the catalyst ink in g; $C_{P(ci)}$ is the specific heat capacity of the catalyst ink in J g^{-1} K^{-1}; $(dT/dt)_{t=0}$ is the slope at $t = 0$ in K s^{-1}.

In this study, the specific heat capacity of water was taken as 4.184 J g^{-1} K^{-1} [22–24] (as 76% (w/w) of water was present in the catalyst ink samples) and ultrasonic powers (P_T) are quoted as W or otherwise stated.

NB: Pollet et al. [4,17] showed, with the aid of mathematical models based on mass-balance equations and using the *quasi-reversible* redox couple $Fe(CN)_6^{3-}/Fe(CN)_6^{4-}$ as an electrochemical model, that a *Levich-like* equation relating the limiting current, the inverse square root of the electrode radius and the inverse square root of the electrode–horn distance, the transmitted ultrasonic power may be generated for ultrasonic frequencies of 20 and 40 kHz (probe systems only and at 298 K) using Eq. (8) also known as the Pollet equation [3,8]:

$$I_{lim} = 0.84nFAD_o^{2/3}\nu^{-1/6}r_e^{-1/2}d^{-1/2}C^*\Psi^{1/2} \quad (8)$$

where I_{lim} is the limiting current (A), n is the number of electrons transferred during the electrochemical process, F is the Faraday constant (C mol^{-1}), A is the electrode area (cm^2), D_o is the diffusion coefficient (cm^2 s^{-1}) of the electroactive species, d is the ultrasonic horn–electrode distance (cm), ν is the kinematic viscosity (cm^2 s^{-1}), r_e is the working electrode radius (cm), C^* is the bulk concentration of the electroactive species (mol cm^{-3}) and Ψ is the ultrasonic intensity (W cm^{-2}) [ultrasonic power transmitted (P_T, W) divided by the ultrasonic horn tip area (A_{uht}, cm^2) i.e. $\Psi = P_T/A_{uht}$].

Fig. 4(a) shows T vs. t plots at various electric output powers, and curve fitting calculations confirm a 6th order polynomial form for all plots. Fig. 4(b) shows that as the electric output power (P_e) delivered by the ultrasonic generator increases, the transmitted ultrasonic power (P_T) also increases for both ultrasonic equipment used. From Fig. 4 and using Eqs. (4)–(7), the ultrasonic powers were 1.82 W for the ultrasonic bath and 3.03 W, 6.70 W, 12.23 W and 15.49 W for the ultrasonic probe corresponding to 20%, 40%, 60% and 80% power setting of the device. However, it was noted that

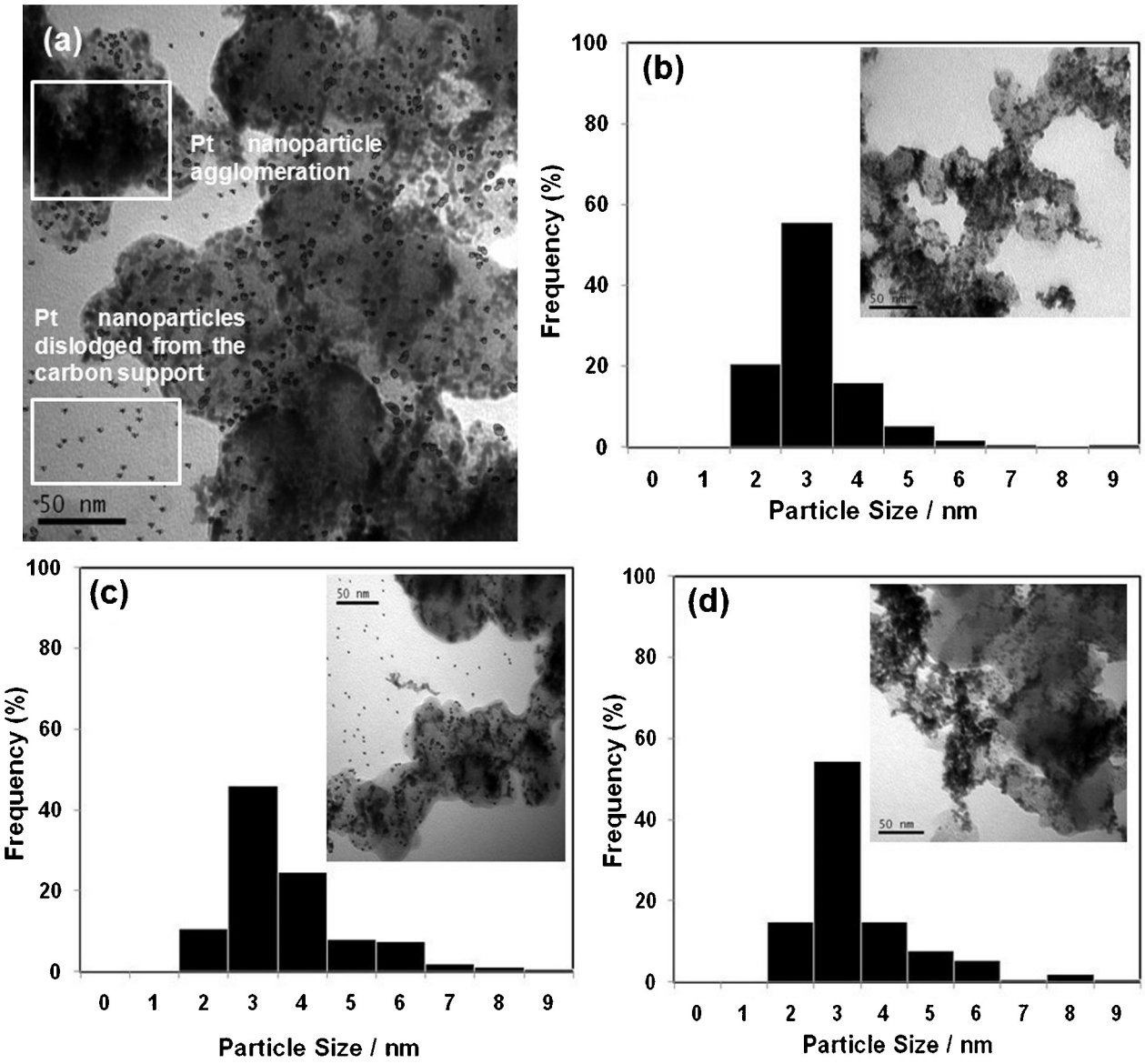

Fig. 6. (a) TEM image of an *E-TEK* sample irradiated (20 kHz) for 30 min at 6.70 W (20 kHz) and at (298 ± 1) K; particle size histograms and TEM images (inset) for the *E-TEK* samples irradiated at 12.23 W (20 kHz) and at (298 ± 1) K (b) for 10 min; (c) 20 min; (d) 120 min.

the use of the ultrasonic probe at 15.49 W (80% power) resulted in excessive agitation and even splashing of the solution and was therefore excluded from tests with the catalyst ink.

3.2. The effect of ultrasound on catalyst inks

3.2.1. E-TEK Catalysts

For the *E-Tek* catalyst samples, the catalyst inks treatment was found to have a significant effect on *ECSA* as shown in Fig. 5(a). Table 1 shows values of the average diameter of Pt nanoparticles, their surface areas, *ECSA*s and utilizations under silent, high-shear mixed (no ultrasound) and ultrasonicated conditions at various durations. It was found that at least 30 min of ultrasonication was required to produce homogeneous catalyst dispersions yielding reproducible *ECSA* values. Catalyst inks ultrasonicated for shorter durations exhibited poor reproducibility in *ECSAs*, regardless of the ultrasonic frequency and power employed. From the data, we infer that the main action of ultrasound in the irradiation time range of 0–30 min is to aid the homogeneity of the catalyst ink via mixing and possible de-agglomeration of the catalyst particles caused by the implosion of cavitation bubbles (see later). Note that *ECSAs* determined at $t = 0$ s (not shown here) i.e. in the absence of high-shear mixing and ultrasound were found to be inconsistent with an error from one sample to another of ±20–50%, indicating that mixing is required to obtain homogenous samples.

The *E-Tek* catalyst ink samples treated in the ultrasonic bath (40 kHz, 1.82 W) exhibited consistently higher *ECSAs* than those treated with the ultrasonic probe (20 kHz, 3.03–12.23 W), with a maximum *ECSA* of 83 $m^2 g^{-1}$ found after 30 min of ultrasonication. For the catalyst inks ultrasonicated using the ultrasonic bath (1.82 W), and for those treated with the ultrasonic probe at the two lower ultrasonic powers (3.03 W and 6.70 W), *ECSAs* were found to decrease with increasing ultrasonication time beyond 30 min. Fig. 5(b) shows plots of *ECSAs* vs. ultrasonic powers at various irradiation times. It is evident from the figure that the *ECSA* decreases significantly with increasing ultrasonic power with, for some cases, a maximum decrease in *ECSA* of ca. 50% across the ultrasonic power range used. This observation can be ascribed to one or more of the following effects:

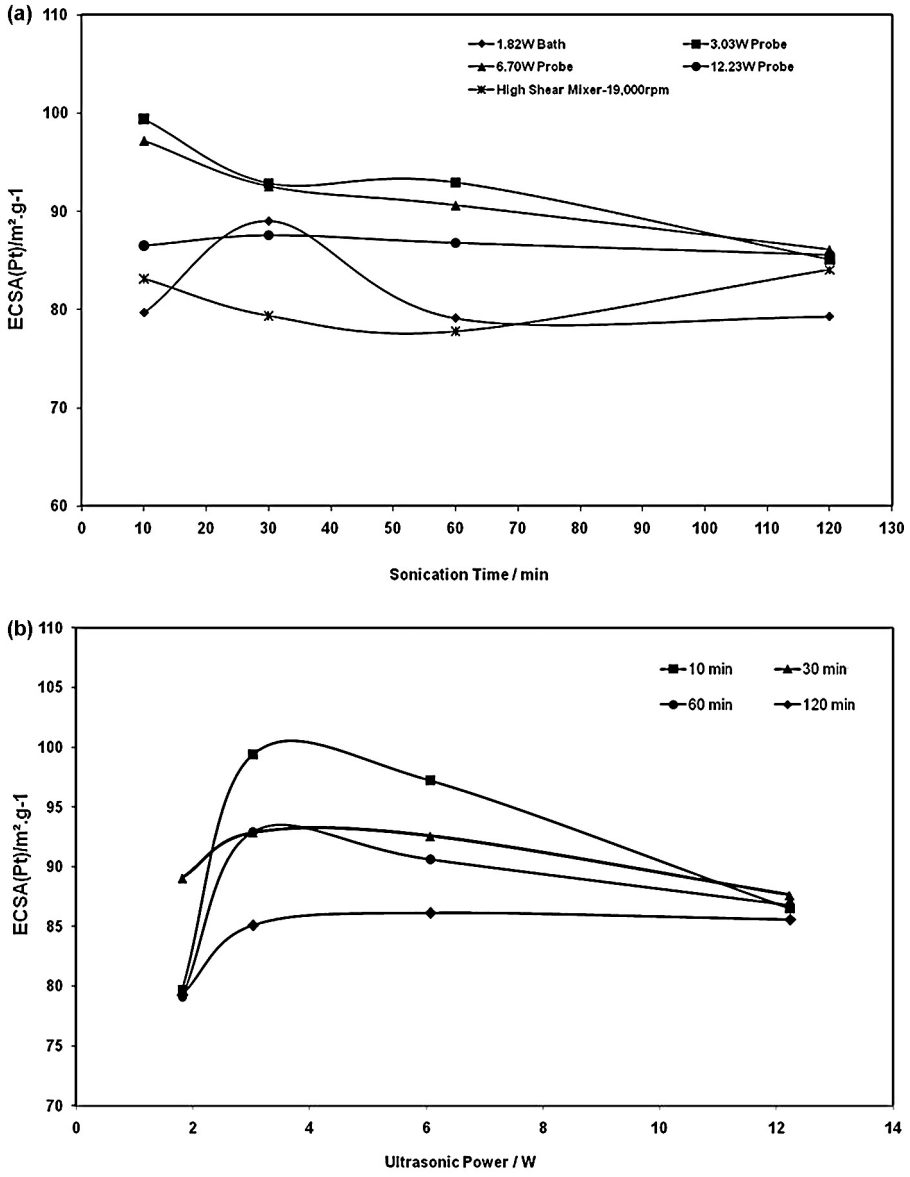

Fig. 7. (a) Plots of *ECSAs* vs. *ultrasonication time* at the ultrasonic frequencies (20 and 40 kHz), at various ultrasonic powers and for high-shear mixing (19,000 rpm, no ultrasound – silent) of *TKK* samples – *ECSA* values (at least 3 replicates) were determined from cyclic voltammograms experiments recorded at 25 mV s^{-1} in 0.1 M $HClO_4$ (not shown here) and at (298 ± 1) K; (b) plots of *ECSAs* vs. *ultrasonic powers* at various ultrasonication times for the *TKK* samples.

(i) It is possible that physical detachment of Pt nanoparticles from the carbon support under ultrasonication may occur such that they are expelled and embedded within the Nafion® matrix upon drying, thus becoming electrically isolated and unavailable for electron transfer. Thus, it is proposed that Pt particle detachment results from physical degradation of the carbon support, mainly due to erosion [4] induced by violent implosion of cavitation bubbles producing jets of liquid exceeding 20 m s^{-1} [17] directed onto the carbon surface and Pt/carbon interfaces. Indeed, for samples treated for longer periods and/or high ultrasonic powers, significant detachment of Pt nanoparticles from the carbon support was observed in TEM images [Fig. 6(a)]. This finding suggests that for the *E-tek* catalyst, the adhesion of Pt on the carbon support is weak.

(ii) It is also possible that partial or complete sonochemical dissolution of platinum may occur [3]. Radziuk et al. [25] showed that the ultrasonic treatment affects the crystal structure of platinum nanoparticles in aqueous solutions. They found that the Pt nanoparticle crystallinity is reduced strongly by ultrasonication up to its complete disappearance, and that this effect can be mitigated through the introduction of protective ligands such as polyvinylpyrrolidone (PVP) and ethylene glycol (EG). In this work, the Pt nanoparticles supported on carbon do not have any 'protection' and are directly exposed to the aqueous solution. According to Radziuk et al. [25], dissolution of Pt proceeds easily under intensive ultrasonication of this kind. The presence of soluble Pt species leads to an increase in the rate of Pt particle growth via Ostwald ripening, and evidence for this effect can be seen in Fig. 6(b) and (c), in which the fraction of large Pt particles increases for longer ultrasonication times.

(iii) It is plausible that Pt nanoparticle agglomeration occurs within the catalyst ink sample, as shown in Fig. 4(a), caused by weakening of the metal–support interaction, along with the action of *Van der Waals* forces.

These combined effects lead to losses in *ECSAs* between 10 and 15% after 120 min sonication compared to *ECSA* values at 30 min

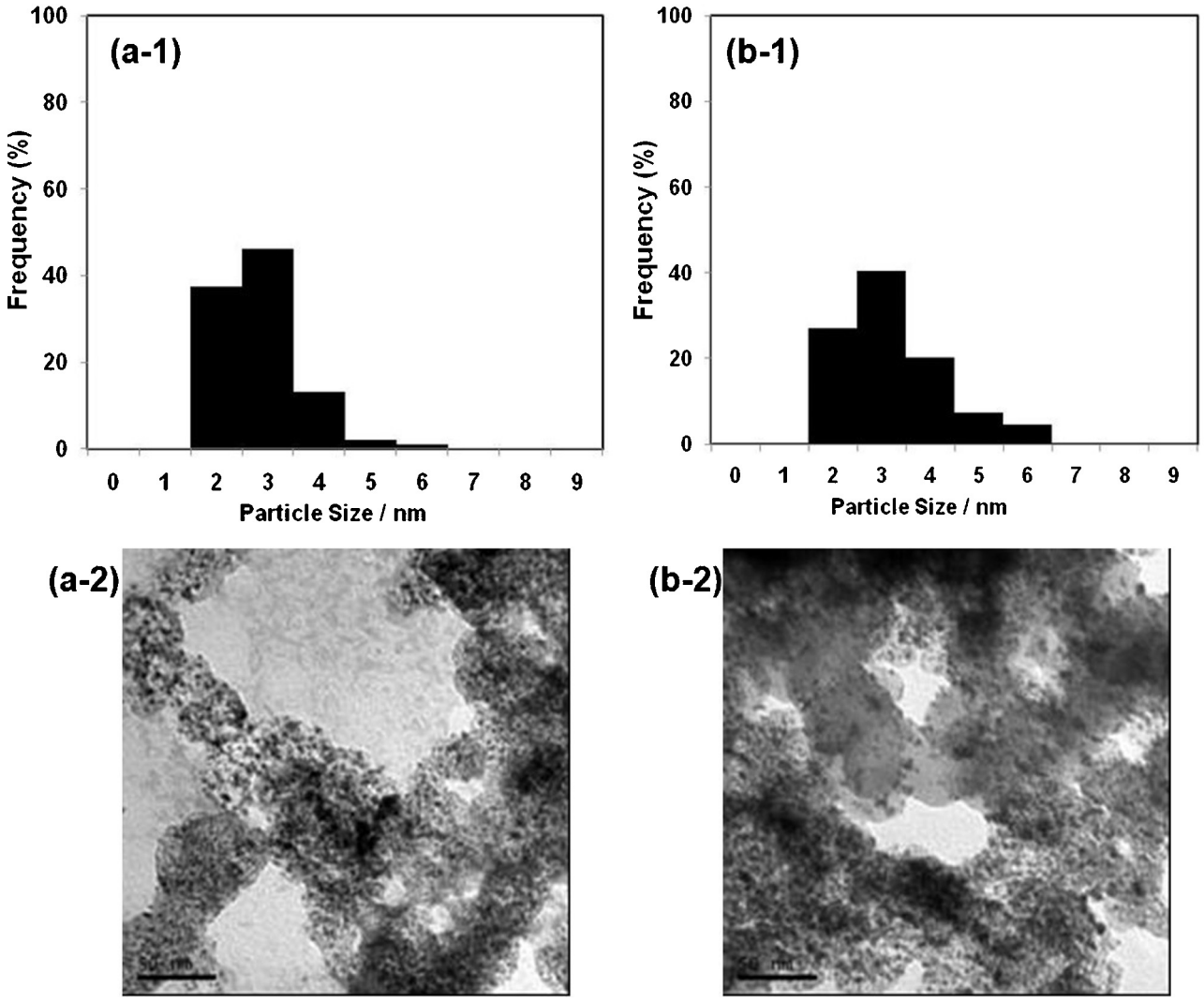

Fig. 8. *TKK* samples treated in the ultrasonic bath [40 kHz, 1.82 W, (298 ± 1) K]: (a-1) particle size histogram and (a-2) TEM image of a *TKK* sample ultrasonicated for 30 min; (b-1) particle size histogram and (b-2) TEM image of a *TKK* sample ultrasonicated for 120 min.

irradiation, and also account for the direct correlation observed between ultrasonic power and *ECSA* as shown in Fig. 3(b).

Interestingly, catalyst ink samples ultrasonicated at high ultrasonic powers (12.23 W) yield poor *ECSA* values compared to those obtained at 3.03 W and 6.7 W in the range of ultrasonication times employed, although the values increase by nearly two-fold after 120 min [Fig. 5(a)]. This could be possibly due to: (i) the slow de-aggregation of Pt nanoparticles caused by the implosion of cavitation bubbles on the Pt nano-aggregates; and/or (ii) nucleation of new Pt nanoparticles following sonochemical reduction of dissolved Pt species, leading to an increase in *ECSA*. In support of this hypothesis, Okitsu et al. [26] found that four pathways were possible for the sonochemical reduction of Pt(II) to produce nano-size metal particles (ca. 5 nm). Based on this finding, Mizukoshi et al. [27] studied the preparation of Pt nanoparticles by the sonochemical reduction of Pt(II) in the presence of sodium dodecyl sulfate (SDS). The average diameters of the stable Pt nanoparticles formed were 2.6 ± 0.9 nm. They attributed the formation of Pt nanoparticles to the reducing species (radicals) generated by water sonolysis induced by cavitation which also followed the mechanisms described by Nagata et al. [28]. He [29] and Mizukoshi et al. [30] also reported that two types of reducing radicals induced by sonolysis and thermolysis are involved in a two-step mechanism where Pt nanoparticles (1–3 nm) are formed: step (1) – Pt(IV) ions to Pt(II) ions and step (2) – Pt(II) ions to Pt(0). In our work here, the harsh ultrasonication treatment at 12.23 W possibly leads to a sonochemical reduction process in the solution, which could explain the small increase in the number of Pt nanoparticles in the range 2–4 nm compared to the samples treated for 10 min as shown in Fig. 6(d).

For the samples prepared using the high shear mixer at a speed of 19,000 rpm, the *ECSA* values measured are considerably lower compared to the ultrasonicated samples [Fig. 3(a)]. The maximum *ECSA* (45 $m^2\ g^{-1}$) was achieved after 60 min of mixing. This low *ECSA* value could possibly be due to the inadequate dispersion of Pt nanoparticles and the significant presence of larger agglomerates. This was confirmed by TEM images (not shown here), which showed that the high shear mixer did not cause any dislodgement of Pt nanoparticles from the carbon support and larger agglomerates were observed.

3.2.2. TKK catalysts

The *TKK* catalyst ink samples were found to have higher physical surface areas (up to 96.94 ± 2.18 $m^2\ g^{-1}$) as shown in Table 2 than the *E-TEK* catalyst ink samples (Table 1), and *ECSA* values were correspondingly higher in general. Fig. 7(a) shows the *ECSA*

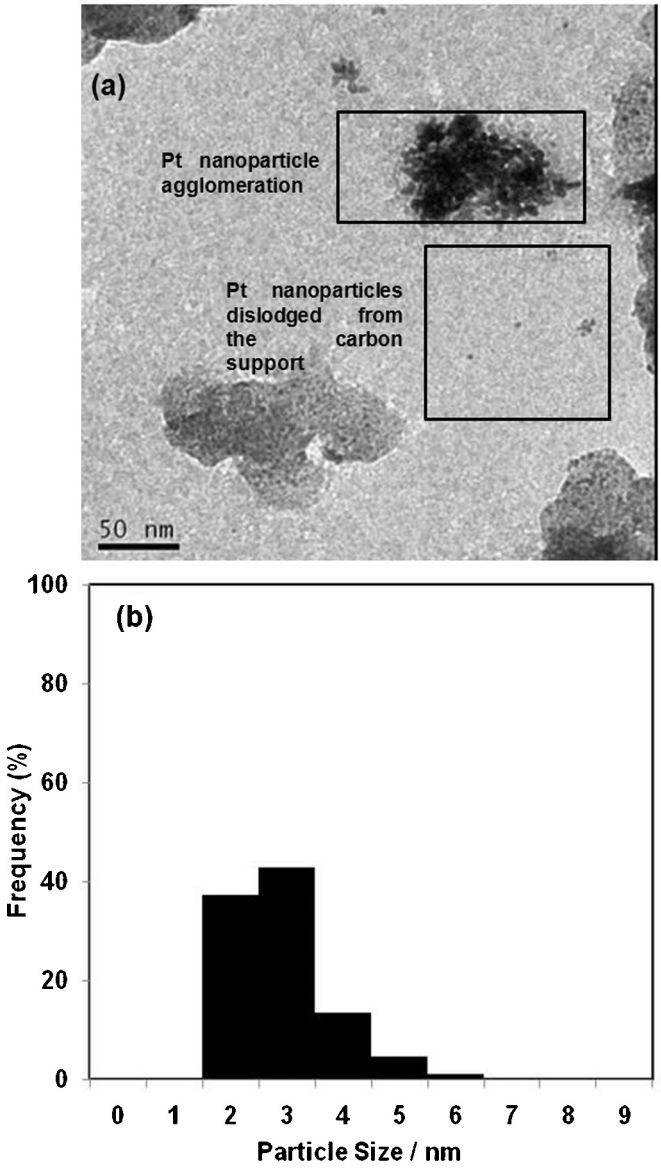

Fig. 9. (a) TEM image and (b) particle size histogram for a *TKK* sample ultrasonicated (20 kHz) for 120 min at 12.23 W and at (298 ± 1) K.

values for all *TKK* samples after ultrasonic treatment. Interestingly, whereas the *E-TEK* catalyst required at least 30 min of ultrasonic treatment for reproducible *ECSAs*, catalyst inks prepared from the *TKK* catalyst generally gave reproducible results after as little as 10 min of ultrasonication, with the exception of samples treated with the ultrasonic bath (40 kHz, 1.82 W), for which at least 30 min of ultrasonication was still required. The more facile homogenisation may indicate less extensive initial agglomeration of the *TKK* catalyst powder or more favourable carbon surface chemistry for forming an aqueous dispersion.

In contrast with the *E-TEK* catalyst ink samples, the best *ECSA* values for the *TKK* samples were obtained for samples treated with the ultrasonic probe (100 $m^2\ g^{-1}$ after 5 min sonication at 20 kHz and at 6.70 W). Samples treated using the ultrasonic bath gave considerably lower *ECSAs* on average than those treated with the ultrasonic probe as shown in Fig. 7(a). Similarly to the *E-TEK* catalyst ink samples, the *ECSAs* of the *TKK* catalyst ink samples were generally found to decrease with increasing ultrasonication time. However, this decrease (observed up to 120 min of ultrasonication) was typically <10%, compared with 10–15% loss observed for the

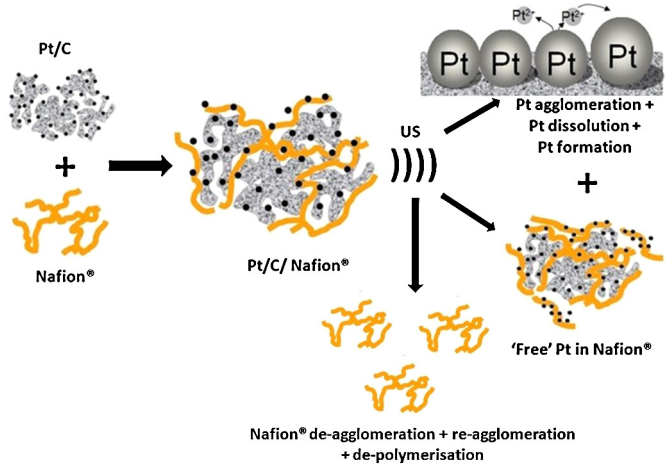

Fig. 10. Schematic mechanism(s) for ultrasonic treatment of catalyst inks (*Pt/C/Nafion®*).

E-TEK catalyst ink samples under similar conditions. The size distributions in Fig. 8(b-1) reveal a significant increase in Pt particle size after 120 min of ultrasonication for samples treated using the ultrasonic bath (compared to the size distributions in Fig. 8(a-1) for samples ultrasonicated for 30 min), which may suggest that Pt dissolution and particle growth via *Ostwald* ripening remain active degradation mechanisms for the *TKK* catalyst at low-power ultrasonic treatments. However, the degree of agglomeration appears largely unchanged, together with a negligible number of detached Pt particles as shown in Fig. 8(a-2) and (b-2). Therefore, we posit that for low-power ultrasonic treatments, the *TKK* catalyst is more 'resistant' to cavitational effects leading to de-agglomeration and particle detachment mechanisms as proposed earlier. In other words, the adhesion of Pt particles on the carbon support for the *TKK* catalyst is strong.

ECSA values for samples ultrasonicated at high ultrasonic powers (up to 12.23 W) were consistently lower than those found at low ultrasonic powers using the ultrasonic probe operating at 20 kHz [Fig. 7(a)]. The *ECSA* values also displayed little variations with increasing ultrasonication times, remaining at around 87 $m^2\ g^{-1}$ for all exposure times. Fig. 9(a) shows that Pt particle detachment and agglomeration become significant degradation modes for the *TKK* catalyst at high ultrasonic powers. From Fig. 9(b), it can be observed that there is a small but significant increase in the number of Pt particles in the very small (2–3 nm) and rather large (5–7 nm) size ranges during ultrasonic treatment at 12.23 W and up to 120 min. The increase in the number of smaller particles suggests that, similarly to the *E-TEK* catalyst ink samples, there is a possible sonochemical reduction/nucleation mechanism for the deposition of new Pt particles at high ultrasonic powers. This effect is counteracted by *Ostwald* ripening, agglomeration and Pt detachment such that the *ECSA* values remain largely unchanged throughout ultrasonication.

From Fig. 7(b), it is clear that the optimal *ECSA* values are obtained at ~3.03 W (ultrasonic probe 20 kHz) suggesting that this ultrasonic power allows maximum dispersion of the catalyst ink whilst minimising degradation effects.

Fig. 10 shows possible mechanism(s) for ultrasonic treatment of catalyst inks (*Pt/C/Nafion®*).

4. Conclusions

This study reports the effects of ultrasound on catalyst inks prepared from commercial *E-TEK* and *TKK* Pt/C electrocatalysts. It was found that irradiation treatments by using either an

ultrasonic bath or an ultrasonic probe operating at 1.82 W and 3.03 W respectively are helpful for catalyst dispersion and thus in improving catalytic activity via an increase in *ECSA*. However, aggressive ultrasonication treatment, e.g. 12.23 W (ultrasound probe), results in lower *ECSA* values mainly due to possible ultrasound-induced ablation, agglomeration and dissolution of Pt nanoparticles. The authors strongly suggest that: (i) care should be taken when ultrasonicating catalyst inks whereby the ultrasonic parameters such as frequency, power and duration affect the final ink composition and rheology, and therefore its electrochemical performance, (ii) ultrasonic equipment, frequencies, powers and durations should be reported in investigations using ultrasound, (iii) the catalyst ink temperature should be monitored and regulated during the course of the experiment, and (iv) high-shear mixing of the catalyst inks using rotor-stator mixers at high rotation speed in silent conditions should be performed, analysed and compared to ultrasonicated samples for consistency and comparison purposes between studies. Finally from our investigation and in general, shorter irradiation times suffice in order to obtain very good homogenisation and dispersion of the catalyst ink.

Acknowledgements

The authors would like to thank members of the University of Birmingham Centre for Hydrogen and Fuel Cell Research: Paula M. Mendes, Oliver J. Curnick and Shangfeng Du who were involved in some of the experimental work and in the proof-reading of this article. The authors are also grateful for Cheng Peng's initial work on this study.

References

[1] S. Litster, G. McLean, PEM Fuel Cell Electrodes, J. Power Sources 130 (2004) 61.
[2] J.-H. Wee, K.-Y. Lee, S.H. Kim, Fabrication Methods for Low-Pt-loading Electrocatalysts in Proton Exchange Membrane Fuel Cell Systems, J. Power Sources 165 (2007) 667.
[3] B.G. Pollet, The Use of Ultrasound for the Fabrication of Fuel Cell Materials, Int. J. Hydrogen Energy 35 (21) (2010) 11986.
[4] B.G. Pollet (Ed.), Power Ultrasound in Electrochemistry: From Versatile Laboratory Tool to Engineering Solution, John Wiley & Sons, Ltd, Chichester, UK, 2012.
[5] J. Thorneycroft, S.W. Barnaby, Minutes of the Proceedings (Institution of Civil Engineers), Inst. Civil Eng. 122 (1895) 51.
[6] L. Rayleigh, On the Pressure Developed in a Liquid during the Collapse of a Spherical Cavity, Philos. Mag. 34 (199-04) (1917) 94.
[7] W.T. Richards, A.L. Loomis, The Chemical Effects of High Frequency Sound Waves I. A Preliminary Survey, J. Am. Chem. Soc. 49 (1927) 3086.
[8] I. Takahashi, S.S. Kocha, Examination of the Activity and Durability of PEMFC catalysts in Liquid Electrolytes, J. Power Sources 195 (19) (2010) 6312.
[9] Y. Garsany, O.A. Baturina, K.E. Swider-Lyons, S.S. Kocha, Experimental Methods for Quantifying the Activity of Platinum Electrocatalysts for the Oxygen Reduction Reaction, Anal. Chem. 82 (2010) 6321.
[10] H. Momand, The Effect of Ultrasound on Nafion® Polymer Exchange Membrane Fuel Cells (PEMFCs), The University of Birmingham, 2013 (M.Res. Thesis).
[11] E.W. Flosdorf, L.A. Chambers, The Chemical Action of Audible Sound, J. Am. Chem. Soc. 55 (1933) 3051.
[12] A. Weissler, Depolymerization by Ultrasonic Irradiation: The Role of Cavitation, J. Appl. Phys. 21 (2) (1950) 171–173.
[13] P.A.R. Glynn, B.M.E. Van der Hoff, The Rate of Degradation by Ultrasonation of Polystyrene in Solution, J. Macromol. Sci., Part A: Pure Appl. Chem. 8 (2) (1974) 429.
[14] C.E. Gall, B.M.E. Van der Hoff, A Method for Following Changes in Molecular Weight Distributions of Polymers on Degradation: Development and Comparison with Ultrasonic Degradation Experiments, J. Macromol. Sci., Part A: Pure Appl. Chem. 11 (9) (1977) 1739.
[15] G.J. Price, P.J. West, P.F. Smith, Control of Polymer Structure using Power Ultrasound, Ultrason. Sonochem. 1 (1994) 51.
[16] K.S. Suslick, G.J. Price, Applications of Ultrasound to Materials Chemistry, Ann. Rev. Mater. Sci. 29 (1999) 295.
[17] B.G. Pollet, J.-Y. Hihn, M.-L. Doche, J.P. Lorimer, A. Mandroyan, T.J. Mason, Transport Limited Current Close to an Ultrasonic Horn: Equivalent Flow Velocity Determination, J. Electrochem. Soc. 154 (10) (2007) E131–E138.
[18] H.A. Gasteiger, S.S. Kocha, B. Sompalli, F.T. Wagner, Activity Benchmarks and Requirements for Pt, Pt-alloy, and non-Pt Oxygen Reduction Catalysts for PEMFCs, Appl. Catal. B: Environ. 56 (56) (2005) 9–35.
[19] O.J. Curnick, B.G. Pollet, P.M. Mendes, Nafion®-stabilised Pt/C Electrocatalysts with Efficient Catalyst Layer Ionomer Distribution for Proton Exchange Membrane Fuel Cells, RSC Adv. 2 (22) (2012) 8368.
[20] S. Calvin, S.X. Luo, C. Caragianis-Broadbridge, J.K. McGuinness, E. Anderson, A. Lehman, K.H. Wee, S.A. Morrison, L.K. Kurihara, Comparison of Extended X-ray Absorption Fine Structure and Scherrer Analysis of X-ray Diffraction as Methods for Determining Mean Sizes of Polydisperse Nanoparticles, Appl. Phys. Lett. 87 (2005) 233102.
[21] V. Zin, B.G. Pollet, M. Dabala, Sonoelectrochemical (20 kHz) Production of Platinum Nanoparticles from Aqueous Solutions, Electrochim. Acta 54 (2009) 7201.
[22] T.J. Mason, J.P. Lorimer, D.M. Bates, Y. Zhao, Dosimetry in Sonochemistry: The Use of Aqueous Terephthalate Ion as a Fluorescence Monitor, Ultrason. Sonochem. 1 (2) (1994) S91.
[23] T.J. Mason, A.J. Cobley, J.E. Graves, D. Morgan, New Evidence for the Inverse Dependence of Mechanical and Chemical Effects on the Frequency of Ultrasound, Ultrason. Sonochem. 18 (1) (2011) 226.
[24] M.A. Margulis, I.M. Margulis, Calorimetric Method for Measurement of Acoustic Power Absorbed in a Volume of a Liquid, Ultrason. Sonochem. 10 (2003) 343.
[25] D. Radziuk, H. Mohwald, D. Shchukin, Ultrasonic Activation of Platinum Catalysts, J. Phys. Chem. C 112 (2008) 19257.
[26] K. Okitsu, Y. Mizukoshi, H. Bandow, Y. Maeda, T. Yamamoto, Y. Nagata, Formation of Noble Metal Particles by Ultrasonic Irradiation, Ultrason. Sonochem. 3 (3) (1996) S249.
[27] Y. Mizukoshi, R. Oshima, Y. Maeda, Y. Nagata, Preparation of Platinum Nanoparticles by Sonochemical Reduction of the Pt(ii) ion, Langmuir 15 (8) (1999) 2733.
[28] Y. Nagata, Y. Watanabe, S. Fujita, T. Dohmaru, S.J. Taniguchi, Formation of Colloidal Silver in Water by Ultrasonic Irradiation, J. Chem. Soc. Chem. Commun. (1992) 1620.
[29] Y. He, K. Vinodgopal, M. Ashokkumar, F. Griese, Sonochemical Synthesis of Ruthenium Nanoparticles, Res. Chem. Intermed. 32 (8) (2006) 709.
[30] Y. Mizukoshi, E. Takagi, H. Okuno, R. Oshima, Y. Maeda, Y. Nagata, Preparation of Platinum Nanoparticles by Sonochemical Reduction of the Pt(iv) ions: Role of Surfactants, Ultrason. Chem. 8 (2001) 1.